Report

Cell Reports

Transglutaminase Type 2 Regulates ER-Mitochondria Contact Sites by Interacting with GRP75

Graphical Abstract

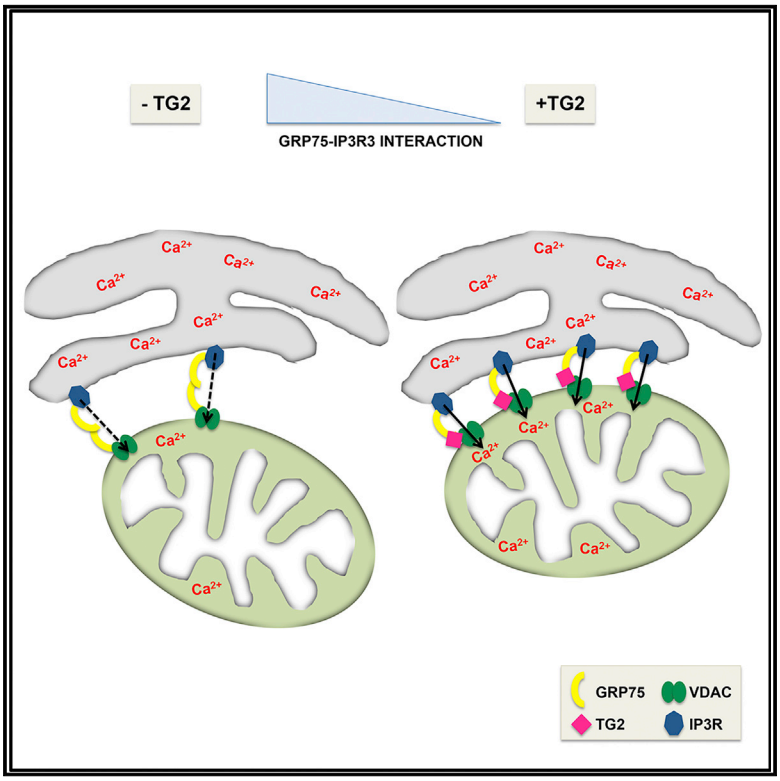

Authors

Manuela D'Eletto, Federica Rossin, Luca Occhigrossi, ..., Paolo Pinton, Michelangelo Campanella, Mauro Piacentini

Correspondence

mauro.piacentini@uniroma2.it

In Brief

TG2 is an enzyme that plays a key role in mitochondria homeostasis. D'eletto et al. found that TG2 interacts with GRP75, a protein localized in mitochondria-associated membranes (MAMs). TG2 regulates the number of ER-mitochondria contact sites and Ca^{2+} flux, suggesting a key regulatory role in MAMs.

Highlights

- TG2 interacts with GRP75 in mitochondria-associated membranes (MAMs)
- TG2 influences the number of ER-mitochondria contact sites
- TG2 regulates the interaction between IP3R3 and GRP75
- TG2 controls ER-mitochondrial Ca^{2+} flux and protein expression in MAMs

D'Eletto et al., 2018, Cell Reports *25*, 3573–3581
December 26, 2018
https://doi.org/10.1016/j.celrep.2018.11.094

CellPress

Cell Reports
Report

Transglutaminase Type 2 Regulates ER-Mitochondria Contact Sites by Interacting with GRP75

Manuela D'Eletto,[1] Federica Rossin,[1] Luca Occhigrossi,[1] Maria Grazia Farrace,[1] Danilo Faccenda,[2] Radha Desai,[2] Saverio Marchi,[3] Giulia Refolo,[4] Laura Falasca,[4] Manuela Antonioli,[4] Fabiola Ciccosanti,[4] Gian Maria Fimia,[4,5] Paolo Pinton,[3] Michelangelo Campanella,[1,2,6] and Mauro Piacentini[1,4,7,*]

[1]Department of Biology, University of Rome "Tor Vergata," Rome 00133, Italy
[2]Department of Comparative Biomedical Sciences, The Royal Veterinary College, University of London, Royal College Street, London NW1 0TU, UK
[3]Department of Morphology, Surgery and Experimental Medicine, Section of Pathology, Oncology and Experimental Biology, Laboratory for Technologies of Advanced Therapies (LTTA), University of Ferrara, Ferrara 44122, Italy
[4]National Institute for Infectious Diseases IRCCS "L. Spallanzani," Rome 00149, Italy
[5]Department of Biological and Environmental Sciences and Technologies (DiSTeBA), University of Salento, Lecce 73100, Italy
[6]UCL Consortium for Mitochondrial Research, Gower Street, London WC1E 6BT, UK
[7]Lead Contact
*Correspondence: mauro.piacentini@uniroma2.it
https://doi.org/10.1016/j.celrep.2018.11.094

SUMMARY

Transglutaminase type 2 (TG2) is a multifunctional enzyme that plays a key role in mitochondria homeostasis under stressful cellular conditions. TG2 interactome analysis reveals an enzyme interaction with GRP75 (glucose-regulated protein 75). GRP75 localizes in mitochondria-associated membranes (MAMs) and acts as a bridging molecule between the two organelles by assembling the IP3R-GRP75-VDAC complex, which is involved in the transport of Ca^{2+} from the endoplasmic reticulum (ER) to mitochondria. We demonstrate that the TG2 and GRP75 interaction occurs in MAMs. The absence of the TG2-GRP75 interaction leads to an increase of the interaction between IP3R-3 and GRP75; a decrease of the number of ER-mitochondria contact sites; an impairment of the ER-mitochondrial Ca^{2+} flux; and an altered profile of the MAM proteome. These findings indicate TG2 is a key regulatory element of the MAMs.

INTRODUCTION

Transglutaminase type 2 (TG2) is the most ubiquitous member of a large group of enzymes that catalyze the Ca^{2+}-dependent posttranslational modification of proteins, including protein-protein cross-linking, incorporation of primary amines into proteins, and glutamine deamination (Piacentini et al., 2011). TG2 possesses more than one catalytic function, and under physiological conditions, the low cytosolic Ca^{2+}concentration does not allow the protein to act as a transamidating enzyme. TG2 can also bind and hydrolyze GTP and acts as a G protein (Begg et al., 2006). Moreover, it has also been reported that TG2 possesses intracellular serine/threonine protein kinase and protein disulfide isomerase (PDI) activity (Hasegawa et al., 2003).

The PDI activity of TG2 has been shown to lead to the post-translational modification of key mitochondrial proteins, and this activity is required for the proper assembly of the respiratory chain complexes (Altuntas et al., 2014). Furthermore, in absence of TG2's PDI activity, we observed an incorrect assembly of mitochondrial ADP/ATP transporter adenine nucleotide translocator 1 (ANT1) (Malorni et al., 2009). We have also recently demonstrated that TG2 is involved in mitophagy, particularly under stressful cellular conditions (Rossin et al., 2014, 2015).

The analysis of TG2's interactome has revealed that TG2 interacts with several proteins belonging to different functional categories, such as chaperones, mitochondrial proteins, metabolic, and cytoskeletal (Altuntas et al., 2015; Diaz-Hidalgo et al., 2016; D'Eletto et al., 2018). Among these, particularly interesting is GRP75 (glucose-regulated protein75), also known as mortalin, a molecular chaperone belonging to the Hsp70 family (Wadhwa et al., 1993a). Despite being predominantly localized in the mitochondria, GRP75 has also been found in other subcellular compartments (Wadhwa et al., 1993b). It has been demonstrated that GRP75 tethers the N-terminal domain of the IP3 receptors to VDAC1, generating a molecular bridge that enhances the Ca^{2+} accumulation in mitochondria by stabilizing conformations or the coupling of the two receptors (Szabadkai et al., 2006). The IP3R-GRP75-VDAC complex is present at the ER-mitochondria interface, the so-called MAMs (mitochondria-associated membranes), where it plays a crucial role in the regulation of the intracellular Ca^{2+} (Patergnani et al., 2011). Basal Ca^{2+} oscillations drive mitochondrial metabolism for the production of ATP and mitochondrial substrates used in anabolic processes (Cárdenas et al., 2010). On the contrary, mitochondrial Ca^{2+} overload can lead to mitochondrial permeability transition pore opening and subsequent cell death (Rizzuto et al., 2012). Dysregulation of Ca^{2+} fluxes is involved in

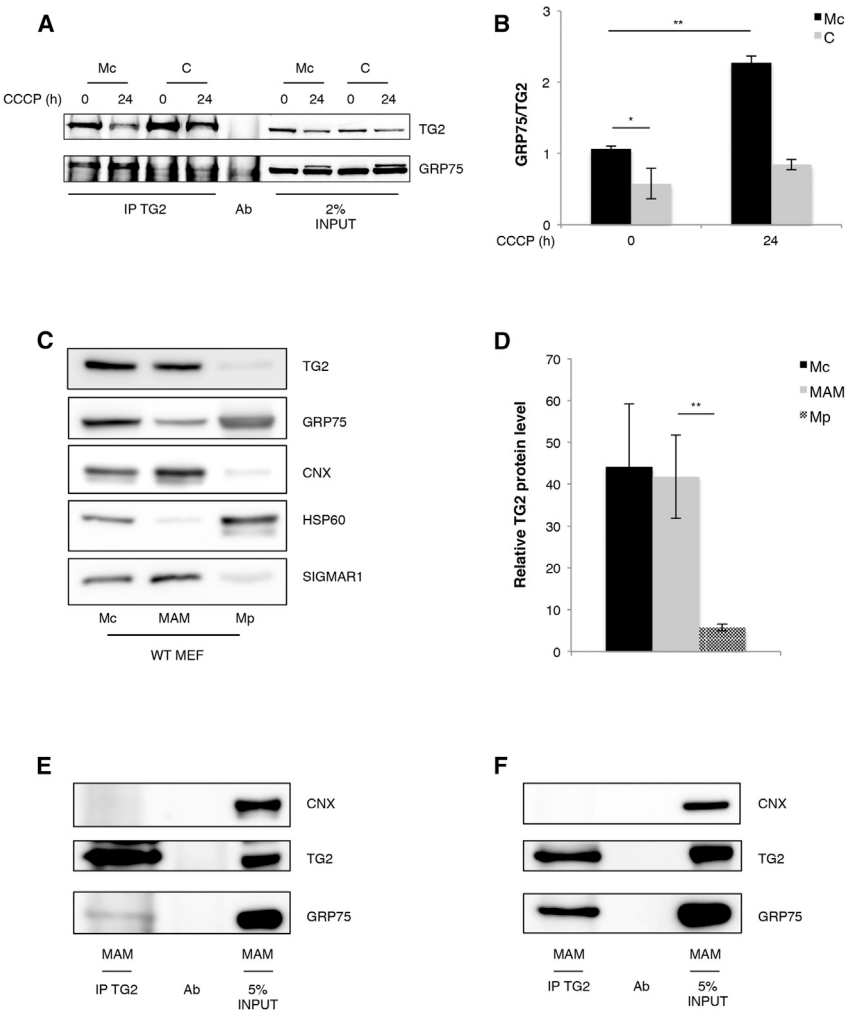

Figure 1. TG2 Interacts with GRP75 in the MAMs

(A) Representative western blot analysis of TG2 and GRP75 in HEK293^{TG2} cells subjected to immunoprecipitation for TG2. After 24 hr of CCCP treatment, cells were fractionated and crude mitochondrial (Mc) and cytosolic (C) proteins were immunoprecipitated using anti-TG2 antibody. Immunoprecipitated and co-immunoprecipitated proteins were separated by SDS-PAGE and immunoblotted using the indicated antibodies. Crude mitochondrial and cytosolic extracts (INPUT) were used as protein control.

(B) Densitometric analysis of the ratio of co-immunoprecipitated GRP75/TG2 in crude mitochondrial and cytosolic extracts. Data are mean ± SEM of 3 independent experiments (*$p < 0.05$; **$p < 0.01$).

(C) Subcellular distribution of TG2 and GRP75 in crude mitochondria (Mc), mitochondria-associated membrane (MAM), and pure mitochondria (Mp) analyzed by western blot analysis. Marker proteins indicate MAMs (SIGMAR1 and CNX) and pure mitochondria (HSP60). All markers are present in the crude mitochondria.

(D) Densitometric analysis of TG2 protein level in the mitochondrial fractions. Data are mean ± SEM of 3 independent experiments (**$p < 0.01$).

(E and F) Immunoblotting analysis of TG2 and GRP75 in HEK293^{TG2} (E) and WT MEF (F) cells subjected to immunoprecipitation for TG2. The cells were sub-fractionated and the MAM fractions were immunoprecipitated using anti-TG2 antibody. CNX was used as loading control for MAM extracts.

several human disorders (Giorgi et al., 2018; Gómez-Suaga et al., 2018).

Considering the role that TG2 plays in mitochondrial homeostasis as well as the involvement of GRP75 protein in ER-mitochondria Ca^{2+} transfer, we studied the interaction of TG2 and GRP75 to shed light on the possible influence of TG2 in the homeostasis of membrane contact sites between the ER and mitochondria.

RESULTS

TG2 Interacts with GRP75 in the MAMs

To characterize the TG2's binding partners, we have recently performed the enzyme interactome analysis by utilizing the tandem affinity purification approach combined with high-performance liquid chromatography (HPLC) and MALDI TOF-TOF mass spectrometry (Altuntas et al., 2015; Antonioli et al., 2017). This analysis showed that TG2 interacts with several proteins located in the endoplasmic reticulum (ER) and mitochondria (Table S1). Among these, we focus our attention on the heat shock 70 kDa protein 9B precursor, also known as GRP75.

To confirm that TG2 interacts with this putative novel partner, we analyzed the interaction of the enzyme with GRP75. To this aim, TG2 was immunoprecipitated from HEK293 cells reconstituted with wild-type TG2 (HEK293^{TG2}) (D'Eletto et al., 2012). In addition, considering that TG2 is involved in the cellular response to mitochondrial stress (Rossin et al., 2014), we treated HEK293^{TG2} cells with the mitochondrial uncoupler carbonyl cyanide m-chlorophenyl hydrazine (CCCP) for 24 hr. Data reported in Figures 1A and 1B reveal that the interaction between the two proteins occurred both in the crude mitochondrial fraction and in the cytosolic fraction. Interestingly, the interaction of TG2 with GRP75 increases upon CCCP treatment in crude mitochondrial fraction. This result was further confirmed by co-immunoprecipitation of GRP75 in the crude mitochondrial fraction (Figures S1A and S1B).

Considering that GRP75 plays an important role in MAM stabilization (Szabadkai et al., 2006), we verified whether TG2 is present in the MAMs. We performed the subcellular fractionation in wild-type (WT) murine embryonic fibroblast (MEF) cells, and we found that the TG2 present in the crude mitochondrial fraction is localized exclusively at the MAMs, while it is undetectable in the pure mitochondria (Figures 1C and 1D), thus indicating that the interaction of TG2 with GRP75 occurs in the MAM fraction. To verify this hypothesis, we immunoprecipitated TG2 from the MAM protein fractions of HEK293^{TG2} cells and WT MEF (Figures

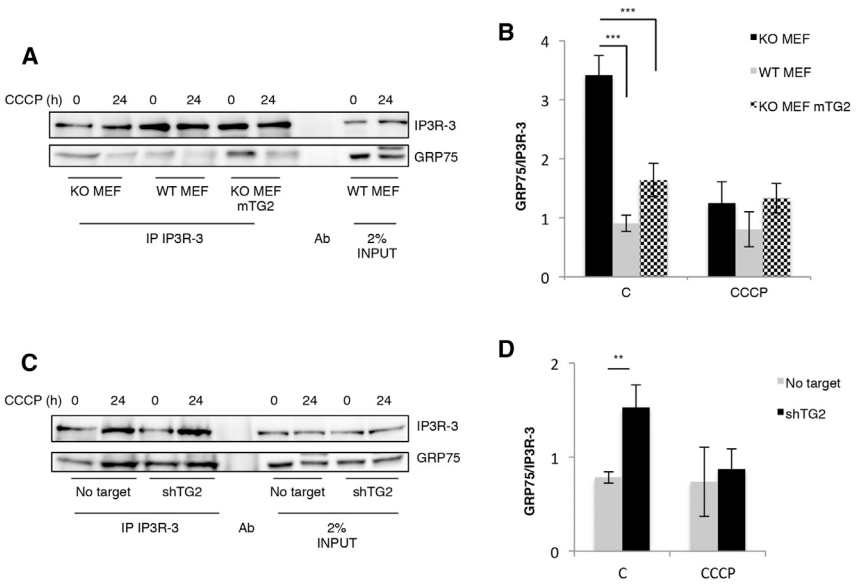

Figure 2. TG2 Influences the Interaction between IP3R-3 and GRP75

(A and C) Representative western blot analysis of IP3R-3 and GRP75 in KO MEF, WT MEF, and KO MEF mTG2 (A) and No target and shTG2 WT MEF (C) subjected to immunoprecipitation for IP3R-3. After 24 hr of CCCP treatment, cells were lysed, and proteins were immunoprecipitated using anti-IP3R-3 antibody. Immunoprecipitated and co-immunoprecipitated proteins were separated by SDS-PAGE and immunoblotted using the indicated antibodies. INPUT, whole cell lysate, was used as protein control.

(B and D) Densitometric analysis of the ratio of co-immunoprecipitated GRP75/IP3R-3 in KO MEF, WT MEF, and KO MEF mTG2 (B) and No target and shTG2 WT MEF (D).

Data are mean ± SEM of 3 independent experiments (**$p < 0.01$; ***$p < 0.001$).

1E and 1F), and the data confirmed that the interaction specifically occurs in the MAM region. Of note, we also confirmed the presence of TG2 in the MAMs *in vivo* in the mouse liver (Figure S2).

TG2 Regulates the Interaction between IP3R3 and GRP75

It has been shown that GRP75 tethers the ligand-binding domain of the IP3 receptors to VDAC1 (Szabadkai et al., 2006). In order to verify whether TG2 could influence the regulation of this complex, we analyzed the interaction of IP3R-3 with GRP75 in presence or absence of TG2. To this aim we co-immunoprecipitated IP3R-3 in WT MEF, knockout (KO) MEF, and KO MEF overexpressing TG2 (KO MEF mTG2) (Figures S3A and S3B), in basal condition and after CCCP treatment. As shown in Figures 2A and 2B, in KO MEF there is an increase of IP3R-3-GRP75 interaction respect to WT MEF in basal condition. Interestingly, this interaction decreases when TG2 was overexpressed, thus suggesting that TG2 could play a role in modulating the functional interaction between these two proteins. To confirm these results, we repeated this experiment by ablating the TG2 in WT MEF using RNA interference (Figures S3C and S3D). The results clearly show that the interaction between IP3R-3 and GRP75, in the presence of TG2, decreases under basal conditions, whereas no significant difference is observed after CCCP treatment (Figures 2C and 2D). These data indicate that the amount of GRP75 present in the IP3R-GRP75-VDAC complex is influenced by the presence of TG2.

TG2 Influences the Number of MAMs

Physiological contacts between ER and mitochondria are defined as involving distances of approximately 10–30 nm (Csordás et al., 2006). Such close connections are required to properly facilitate Ca^{2+} and phospholipid exchange between the two organelles. We used an *in situ* proximity ligation assay (PLA) to detect and quantify the number of contact sites in presence or absence of TG2. WT and KO MEFs were probed with anti-IP3R-3 and anti-VDAC1 primary antibodies followed by hybridization with secondary antibodies coupled to different fluorescent oligonucleotides that hybridize if the distance between two antibody-coupled oligonucleotides is < 40 nm. The analysis of the fluorescence PLA signals (reds dots) showed that in absence of TG2, there are less contact sites, indicating a possible influence of the enzyme in the ER versus mitochondrial membrane interactions (Figures 3A and 3B). We also evaluated PLA signals after 6 hr of CCCP, a treatment known to induce TG2 transamidating activity (Rossin et al., 2015). The analysis of PLA dots after CCCP treatment revealed an increase in the contact sites only in WT MEF (Figure S4A) that was lost after the inhibition of TG2 activity by Z-DON-Val-Pro-Leu-OMe (Z-DON) (Figure S4B) (D'Eletto et al., 2017). We have also analyzed the ER-mitochondrial contact sites with live cell imaging; to this aim the cells were double stained for the ER (green, using ER-Tracker BODIPY) and mitochondria (red, using Mito-Tracker) (Figure 3C), thus allowing the determination of the coefficients of co-localization and overlap between the two signals. The zoomed panel shows more ER-mitochondrial contacts in WT compared to KO MEFs (Figure 3D). To further corroborate these data, we performed transmission electron microscopy (TEM) analysis in WT and KO liver. ER-outer mitochondrial membrane (OMM) apposition was measured considering the following three subsets of ER-OMM distances: closely associated < 30 nm, between 31 and 50 nm, and between 51 and 100 nm. Figures 3E and 3F clearly confirmed that in absence of TG2 the distance between ER and mitochondria increased, indicating an effective structural role of TG2 in the MAMs.

The Lack of TG2 Alters the Protein Expression in the MAMs

The MAM is a subdomain of the ER acting as a central organizer of several metabolic processes, including calcium and apoptotic signaling, synthesis of phospholipids, cholesterol trafficking,

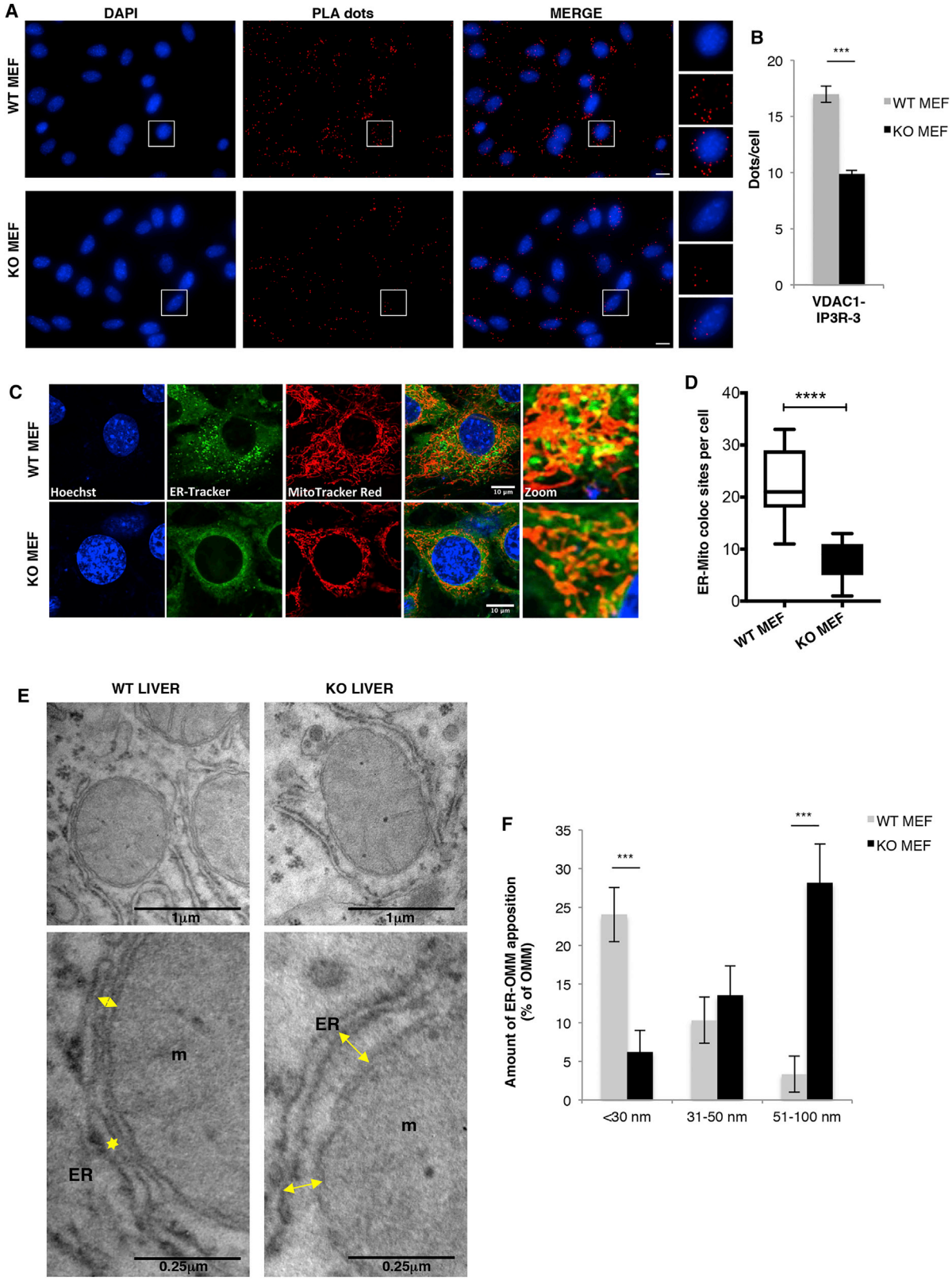

(legend on next page)

and inflammasome signaling (Sassano et al., 2017). Considering the above reported results showing that TG2 is present in the MAMs, where it plays an important structural role regulating the number of contact sites, we decided to analyze whether TG2 could influence the MAM protein composition. As shown in Figure 4, the lack of TG2 drastically changes the protein composition in the MAMs. In fact the protein levels of Mfn2, TBK1, STING, Rab 32, and TSPO decreased in KO MEF with respect to WT MEF in MAM fractions, indicating a possible role of TG2 in the proteome in this region. Interestingly, here we provide the first evidence that TSPO is present in the MAM fraction and its localization is strictly TG2 dependent. It is interesting to note the selective increase in the amount of GRP75 in the MAM fraction of KO MEF.

Effect of TG2 on Mitochondrial Ca^{2+} Uptake

Morphological changes in the mitochondrial network may be linked to alterations in mitochondrial Ca^{2+} uptake pathways (Gatliff et al., 2017). In order to obtain further insight regarding the impact of TG2 on the Ca^{2+} transport efficiency between ER and tethered mitochondria, Ca^{2+} uptake in the organelle was assessed in cells with different levels of TG2 protein (Figure 5). To do so, WT and TG2 overexpressing HEK293 were loaded with fluorescent dyes and elicited via inositol triphosphate (IP3) generating trigger ATP to induce, via the purinergic receptors, mobilization of intracellulary stored Ca^{2+}. The dynamic accumulation of Ca^{2+} in the mitochondria was monitored via the Rhod-2 AM dye, which reported a faster and greater accumulation in presence of forced TG2 expression (Figures 5A and 5B). The analysis on the dynamics of Ca^{2+} was completed using WT and KO MEFs. KO MEF showed a tangibly reduced response when compared to conditions bearing normal TG2 level (Figures 5C and 5D). In these cells, the modulation of mitochondrial Ca^{2+} was corroborated further by using the mitochondria-targeted aequorin (mtAEQ) (Figures S5A and S5B). Interestingly, we also assessed the effect of the TG2 inhibitor Z-DON on the dynamics of mitochondrial Ca^{2+} uptake, which is reported in Figures 5E and 5F. The dataset highlights the effective reduction of Ca^{2+} trafficking in the mitochondria operated by the inhibitor in comparison with untreated conditions. Z-DON treatment is thus superimposable with the effect of TG2 ablation.

DISCUSSION

In this study, we demonstrated that TG2 localizes in the MAMs and its presence in the ER-mitochondria contact site is essential to maintain the correct structural and functional homeostasis of this important cellular regulatory site. We showed that both the MAM proteome profile as well as the Ca^{2+} transport are significantly affected in cells lacking TG2. In the absence of TG2, there is both a decrease in the number and in the architecture of contact sites between ER and mitochondria. In fact, in the absence of TG2, the interaction between these two organelles is largely modified as indicated by the triplicated average distance between them. However, the absence of the enzyme leads to an increased interaction of GRP75 with the IP3R-3 complex. We speculate that this increase represents a compensatory attempt to maintain the contacts between these two organelles. This hypothesis is in line with the increase in the amount of GRP75 detected in the MAM fractions of KO MEF. These data are particularly interesting in light of the fact that the transamidating activity of TG2 is strictly dependent on Ca^{2+} (Tatsukawa et al., 2016). This is relevant considering that the TG2's biochemical activities depend on its open versus closed 3D conformations, which are regulated by the ratio of Ca^{2+} versus GTP levels, thus the enzyme is able to modulate its own activity by regulating the intracellular Ca^{2+} homeostasis. We show here that the inhibition of TG2 by Z-DON, which blocks the enzyme in the inactive open conformation, is able to phenocopy the effects observed in cells lacking the enzyme. This suggests that TG2 in its closed conformation participates in the regulation of the ER-mitochondria contact site as a scaffold. Interestingly, after mitophagy induction by CCCP, there is a specific activation of TG2 transamidating activity on mitochondria, indicating the TG2-dependent posttranslational modification of some mitochondrial proteins upon mitochondrial damage (Rossin et al., 2015).

TG2 plays an important regulatory role in key cellular function such as apoptosis and autophagy. Both these events require the tuning of the intracellular Ca^{2+} level and involve the homeostatic control of mitochondria and the ER, respectively. In fact, excessive uptake of Ca^{2+} by mitochondria can lead to opening of the mitochondrial permeability transition pore and signaling for apoptosis (Rizzuto et al., 2012).

The exquisite localization of TG2 in this cellular compartment in which Ca^{2+} tonicity is particularly high may imply a core redistribution leading to maximize its activity and thus its impact on cellular homeostasis. The cellular ability to handle stress could be well influenced by the TG2 interplays with Ca^{2+} and associated MAM resident mediators. Ablation of the enzyme

Figure 3. TG2 Affects the Number of Contact Sites

(A) Representative images of an *in situ* proximity ligation assay targeting IP3R-3-VDAC1 interactions of WT and KO MEFs. Red dots indicate the location and extent of the interaction. Nuclei were stained with DAPI. Each picture is representative of a typical cell staining observed in 10 fields chosen at random. The scale bar indicates 5 μm.

(B) Quantification of the PLA red fluorescent dots was performed using ImageJ. Data are mean ± SEM of 4 distinct experiments (***$p < 0.001$).

(C) Live cell imaging using confocal microscopy of WT and KO MEFs, nuclei were stained with Hoechst 33342 (blue), endoplasmic reticulum with ER-Tracker BODIPY (green), and mitochondria with MitoTracker Red (red).

(D) Quantification of the ER-mitochondria colocalization sites was performed using ImageJ. Data represent mean ± SEM of 3 different sets of experiments per condition (n = 12–16 cells per coverslip of analysis; ****$p < 0.0001$).

(E and F) Ultrastructural analysis of ER-mitochondria contact (E). Representative TEM images of mitochondria (m) connected to the ER in liver from WT and KO TG2 mice. Higher magnifications highlight ER-OMM distances. Quantification of the relative amount of OMM in contact with the ER for each of the three ER-OMM distance categories (less than 30, between 31 and 50 nm, between 51 and 100 nm) (F).

Bars represent mean ± SEM; n = 50 to 100 mitochondria in 10 fields per condition (***$p < 0.001$).

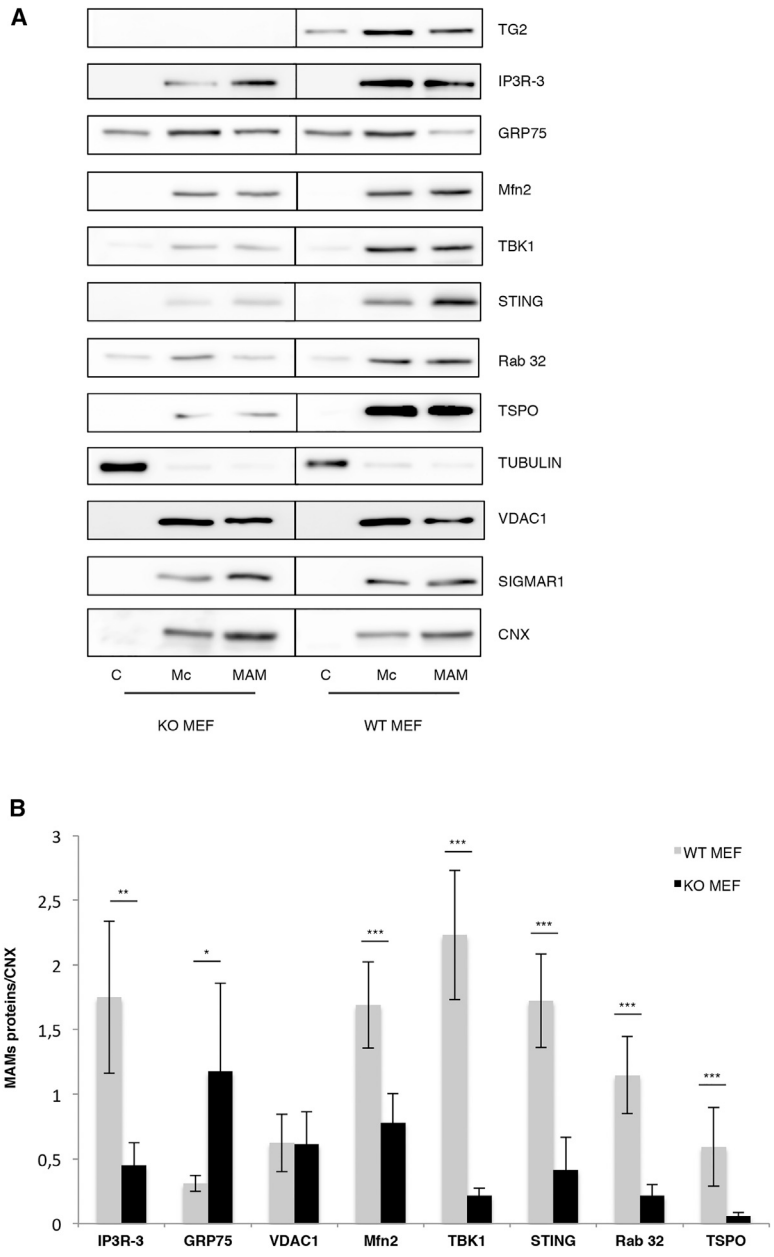

Figure 4. TG2's Effect on the Protein Composition in the MAMs

(A) Representative western blot analysis of chosen proteins in KO and WT MEFs subjected to subcellular fractionation. The cells were fractionated and cytosolic (C), crude mitochondrial (Mc), and MAM proteins were separated by SDS-PAGE and immunoblotted using the indicated antibodies. Tubulin was used as loading control for cytosolic extract. CNX was used as loading control for MAM proteins.

(B) Densitometric analysis of protein levels in MAM normalized to CNX signal.

Data are mean ± SEM of 3 independent experiments (*p < 0.05; **p < 0.01; ***p < 0.001).

is matched by downregulation in the MAM region of the stress response protein TSPO, which negatively regulates mitochondrial Ca^{2+} handling to fuel nicotinamide adenine dinucleotide phosphate hydrogen (NADPH) oxidase production of free radicals (Gatliff et al., 2017). Similarly, we demonstrated the deregulation of MFN2 that regulates the ER morphology by directly tethering the two organelles (de Brito and Scorrano, 2008). The TG2 ablation also leads to a downregulation of Rab 32 in the MAMs where it participates in the control of mitochondrial dynamics (Alto et al., 2002). It has been demonstrated that endogenous and overexpressed Rab 32 localizes to mitochondria and the MAMs in HeLa cells, where it modulates MAM properties and apoptosis onset (Bui et al., 2010). Interestingly, recent reports have demonstrated that cytoplasmic DNA released by microbes and viruses can trigger double-stranded DNA (dsDNA)-sensing pathways, which activate STING (Ishikawa and Barber 2008). STING was found to fractionate with MAMs and mitochondria fractions and then signals to the TANK binding kinase 1 (TBK1)-interferon regulatory factor-3 (IRF3) axis to upregulate type I interferon production (Ishikawa et al., 2009). Both these protein were downregulated in MAMs of TG2 lacking cells, thus confirming the involvement of the enzyme in the infectious diseases outcome (Palucci et al., 2018).

MAM contacts are also required for mitochondrial biogenesis because mitochondrial fission occurs at these contact sites and are one of the districts from which pre-autophagic vesicles are generated (Lee and Yoon 2014; Hamasaki et al., 2013). In keeping with this notion, it is important to mention that TG2 is involved both in autophagy and in mitophagy regulation, and its absence leads to a large number of dysfunctional and fragmented mitochondria with altered morphology and depolarization of the mitochondrial membrane (Rossin et al., 2015; Piacentini et al., 2018).

These data open a new scenario in which TG2 may play a part also in the dynamic regulation of MAMs and its contribution to cellular pathogenesis (Pinton, 2018). On this basis, the data reported in this study contribute to shedding light on the complex role played by TG2 in these essential cellular events under normal and pathological settings.

STAR★METHODS

Detailed methods are provided in the online version of this paper and include the following:

- KEY RESOURCES TABLE
- CONTACT FOR REAGENT AND RESOURCE SHARING
- EXPERIMENTAL MODEL AND SUBJECT DETAILS
  - Cell lines
  - Mice

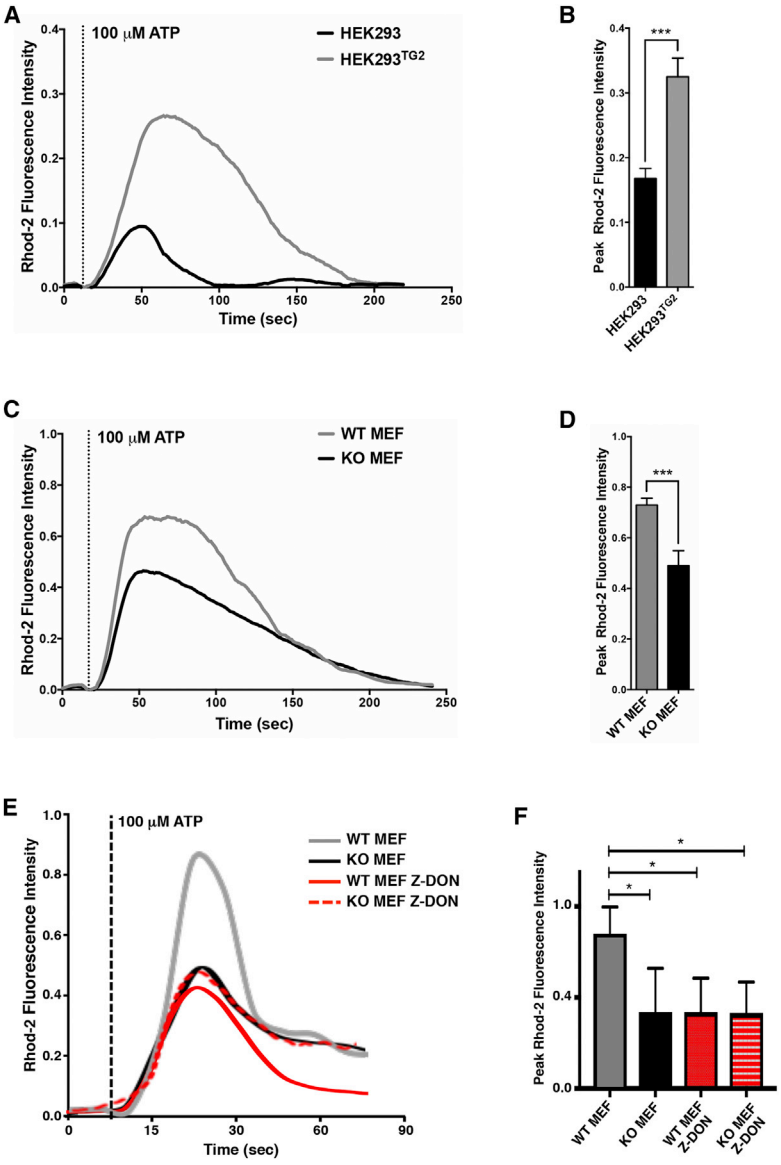

Figure 5. Effect of TG2 on Ca^{2+} Uptake

(A, C, and E) Representative traces of ATP-induced mitochondrial Ca^{2+} uptake in HEK293 (A) and MEFs (C and E). To monitor intramitochondrial Ca^{2+} dynamics, cells were loaded with the mitochondria-specific Ca^{2+} indicator Rhod-2 AM (5 μM) and imaged using a confocal laser-scanning microscope. Cells were challenged with ATP (100 μM) to induce the purinoceptor-dependent emptying of the ER Ca^{2+} stores. Intramitochondrial Ca^{2+} dynamics analysis in WT and KO MEFs in basal condition and after treatment with TG2 inhibitor (Z-DON) (E).

(B, D, and F) Bar charts of average Rhod-2 AM peak fluorescence following administration of ATP in HEK293 (B) and MEFs (D and F).

Data are mean ± SEM of 3 independent experiments (*$p < 0.05$; ***$p < 0.001$).

- METHOD DETAILS
  - Cloning of Murine TG2 gene
  - TG2 knockout reconstitution by retrovirus infection
  - Western blot analysis
  - Subcellular fractionation
  - Co-Immunoprecipitation (Co-IP)
  - Proximity Ligation Assays (PLA)
  - Transmission electron ultrastructural analysis
  - Ca^{2+} signaling analysis
  - Imaging analysis of ER-mitochondria proximity
- QUANTIFICATION AND STATISTICAL ANALYSIS

SUPPLEMENTAL INFORMATION

Supplemental Information includes five figures and one table and can be found with this article online at https://doi.org/10.1016/j.celrep.2018.11.094.

ACKNOWLEDGMENTS

The authors thank Prof. Gerry Melino from the University of Rome "Tor Vergata," Rome, Italy, to have kindly provided TG2 KO mice. P.P. is grateful to Camilla degli Scrovegni for continuous support. This work was supported in part by grants from the AIRC (IG2015-17404 to G.M.F. and IG2018-21880 to M.P.), the Italian Ministry of University and Research (FIRB Accordi di Programma 2011 to M.P. and PRIN 2015 20152CB22L to G.M.F.), the Italian Ministry of Health (Ricerca Corrente and Ricerca Finalizzata RF2010 2305199), Fondazione Fibrosi Cistica (FFC#8/2015 to M.P.), and Regione Lazio (Gruppi di ricerca to M.P.). F.R. was supported by "Fondazione Umberto Veronesi" and AIRC fellowships. The authors also acknowledge the support of the grant from the Russian Government Programme for the Recruitment of the Leading Scientists into the Russian Institutions of Higher Education (14.W03.31.0029 to M.P.). P.P. was supported by the Italian Ministry of Education, University and Research; Telethon (GGP15219/B); the Italian Association for Cancer Research (IG-18624); and local funds from the University of Ferrara. S.M. was supported by "Fondazione Umberto Veronesi" and the Italian Ministry

of Health. M.C. was supported by the Biotechnology and Biological Sciences Research Council (grants BB/M010384/1 and BB/N007042/1); the Medical Research Council (grant G1100809/2); BBSRC LiDO Doctoral Training Partnership; the Petplan Charitable Trust(PPCT); Marie Curie Actions; and the LAM-Bighi Grant Initiative.

AUTHOR CONTRIBUTIONS

M.D. designed and performed most of the experiments. F.R., M.G.F., L.O., S.M., D.F., R.D., G.F., and L.F. performed experiments and analyzed the data. G.M.F., M.A., and F.C. performed the enzyme interactome analysis. M.P. and M.D. wrote the paper. M.P., M.C., and P.P. conceived the project and designed the experiments.

DECLARATION OF INTERESTS

The authors declare no competing interests.

Received: May 15, 2018
Revised: September 20, 2018
Accepted: November 27, 2018
Published: December 26, 2018

REFERENCES

Alto, N.M., Soderling, J., and Scott, J.D. (2002). Rab32 is an A-kinase anchoring protein and participates in mitochondrial dynamics. J. Cell Biol. *158*, 659–668.

Altuntas, S., D'Eletto, M., Rossin, F., Hidalgo, L.D., Farrace, M.G., Falasca, L., Piredda, L., Cocco, S., Mastroberardino, P.G., Piacentini, M., and Campanella, M. (2014). Type 2 Transglutaminase, mitochondria and Huntington's disease: menage a trois. Mitochondrion *19* (*Pt A*), 97–104.

Altuntas, S., Rossin, F., Marsella, C., D'Eletto, M., Diaz-Hidalgo, L., Farrace, M.G., Campanella, M., Antonioli, M., Fimia, G.M., and Piacentini, M. (2015). The transglutaminase type 2 and pyruvate kinase isoenzyme M2 interplay in autophagy regulation. Oncotarget *6*, 44941–44954.

Antonioli, M., Ciccosanti, F., Dengjel, J., and Fimia, G.M. (2017). Methods to Study the BECN1 Interactome in the Course of Autophagic Responses. Methods Enzymol. *587*, 429–445.

Begg, G.E., Carrington, L., Stokes, P.H., Matthews, J.M., Wouters, M.A., Husain, A., Lorand, L., Iismaa, S.E., and Graham, R.M. (2006). Mechanism of allosteric regulation of transglutaminase 2 by GTP. Proc. Natl. Acad. Sci. USA *103*, 19683–19688.

Bonora, M., Giorgi, C., Bononi, A., Marchi, S., Patergnani, S., Rimessi, A., Rizzuto, R., and Pinton, P. (2013). Subcellular calcium measurements in mammalian cells using jellyfish photoprotein aequorin-based probes. Nat. Protoc. *8*, 2105–2118.

Bui, M., Gilady, S.Y., Fitzsimmons, R.E., Benson, M.D., Lynes, E.M., Gesson, K., Alto, N.M., Strack, S., Scott, J.D., and Simmen, T. (2010). Rab32 modulates apoptosis onset and mitochondria-associated membrane (MAM) properties. J. Biol. Chem. *285*, 31590–31602.

Cárdenas, C., Miller, R.A., Smith, I., Bui, T., Molgó, J., Müller, M., Vais, H., Cheung, K.H., Yang, J., Parker, I., et al. (2010). Essential regulation of cell bioenergetics by constitutive InsP3 receptor Ca^{2+} transfer to mitochondria. Cell *142*, 270–283.

Csordás, G., Renken, C., Várnai, P., Walter, L., Weaver, D., Buttle, K.F., Balla, T., Mannella, C.A., and Hajnóczky, G. (2006). Structural and functional features and significance of the physical linkage between ER and mitochondria. J. Cell Biol. *174*, 915–921.

D'Eletto, M., Farrace, M.G., Falasca, L., Reali, V., Oliverio, S., Melino, G., Griffin, M., Fimia, G.M., and Piacentini, M. (2009). Transglutaminase 2 is involved in autophagosome maturation. Autophagy *5*, 1145–1154.

D'Eletto, M., Farrace, M.G., Rossin, F., Strappazzon, F., Giacomo, G.D., Cecconi, F., Melino, G., Sepe, S., Moreno, S., Fimia, G.M., et al. (2012). Type 2 transglutaminase is involved in the autophagy-dependent clearance of ubiquitinated proteins. Cell Death Differ. *19*, 1228–1238.

D'Eletto, M., Farrace, M.G., Piacentini, M., and Rossin, F. (2017). Assessing the Catalytic Activity of Transglutaminases in the Context of Autophagic Responses. Methods Enzymol. *587*, 511–520.

D'Eletto, M., Rossin, F., Fedorova, O., Farrace, M.G., and Piacentini, M. (2018). Transglutaminase type 2 in the regulation of proteostasis. Biol. Chem. Published online June 20, 2018. https://doi.org/10.1515/hsz-2018-0217.

de Brito, O.M., and Scorrano, L. (2008). Mitofusin 2 tethers endoplasmic reticulum to mitochondria. Nature *456*, 605–610.

De Laurenzi, V., and Melino, G. (2001). Gene disruption of tissue transglutaminase. Mol. Cell. Biol. *21*, 148–155.

Diaz-Hidalgo, L., Altuntas, S., Rossin, F., D'Eletto, M., Marsella, C., Farrace, M.G., Falasca, L., Antonioli, M., Fimia, G.M., and Piacentini, M. (2016). Transglutaminase type 2-dependent selective recruitment of proteins into exosomes under stressful cellular conditions. Biochim. Biophys. Acta *1863*, 2084–2092.

Gatliff, J., East, D.A., Singh, A., Alvarez, M.S., Frison, M., Matic, I., Ferraina, C., Sampson, N., Turkheimer, F., and Campanella, M. (2017). A role for TSPO in mitochondrial Ca^{2+} homeostasis and redox stress signaling. Cell Death Dis. *8*, e2896.

Giorgi, C., Marchi, S., and Pinton, P. (2018). The machineries, regulation and cellular functions of mitochondrial calcium. Nat. Rev. Mol. Cell Biol. *19*, 713–730.

Gómez-Suaga, P., Bravo-San Pedro, J.M., González-Polo, R.A., Fuentes, J.M., and Niso-Santano, M. (2018). ER-mitochondria signaling in Parkinson's disease. Cell Death Dis. *9*, 337.

Hamasaki, M., Furuta, N., Matsuda, A., Nezu, A., Yamamoto, A., Fujita, N., Oomori, H., Noda, T., Haraguchi, T., Hiraoka, Y., et al. (2013). Autophagosomes form at ER-mitochondria contact sites. Nature *495*, 389–393.

Hasegawa, G., Suwa, M., Ichikawa, Y., Ohtsuka, T., Kumagai, S., Kikuchi, M., Sato, Y., and Saito, Y. (2003). A novel function of tissue-type transglutaminase: protein disulphide isomerase. Biochem. J. *373*, 793–803.

Ishikawa, H., and Barber, G.N. (2008). STING is an endoplasmic reticulum adaptor that facilitates innate immune signalling. Nature *455*, 674–678.

Ishikawa, H., Ma, Z., and Barber, G.N. (2009). STING regulates intracellular DNA-mediated, type I interferon-dependent innate immunity. Nature *461*, 788–792.

Lee, H., and Yoon, Y. (2014). Mitochondrial fission: regulation and ER connection. Mol. Cells *37*, 89–94.

Malorni, W., Farrace, M.G., Matarrese, P., Tinari, A., Ciarlo, L., Mousavi-Shafaei, P., D'Eletto, M., Di Giacomo, G., Melino, G., Palmieri, L., et al. (2009). The adenine nucleotide translocator 1 acts as a type 2 transglutaminase substrate: implications for mitochondrial-dependent apoptosis. Cell Death Differ. *16*, 1480–1492.

Palucci, I., Matic, I., Falasca, L., Minerva, M., Maulucci, G., De Spirito, M., Petruccioli, E., Goletti, D., Rossin, F., Piacentini, M., and Delogu, G. (2018). Transglutaminase type 2 plays a key role in the pathogenesis of Mycobacterium tuberculosis infection. J. Intern. Med. *283*, 303–313.

Patergnani, S., Suski, J.M., Agnoletto, C., Bononi, A., Bonora, M., De Marchi, E., Giorgi, C., Marchi, S., Missiroli, S., Poletti, F., et al. (2011). Calcium signaling around Mitochondria Associated Membranes (MAMs). Cell Commun. Signal. *9*, 19.

Piacentini, M., D'Eletto, M., Falasca, L., Farrace, M.G., and Rodolfo, C. (2011). Transglutaminase 2 at the crossroads between cell death and survival. Adv. Enzymol. Relat. Areas Mol. Biol. *78*, 197–246.

Piacentini, M., Baiocchini, A., Del Nonno, F., Melino, G., Barlev, N.A., Rossin, F., D'Eletto, M., and Falasca, L. (2018). Non-alcoholic fatty liver disease severity is modulated by transglutaminase type 2. Cell Death Dis. *9*, 257.

Pinton, P. (2018). Mitochondria-associated membranes (MAMs) and pathologies. Cell Death Dis. *9*, 413.

Rizzuto, R., De Stefani, D., Raffaello, A., and Mammucari, C. (2012). Mitochondria as sensors and regulators of calcium signalling. Nat. Rev. Mol. Cell Biol. *13*, 566–578.

Rossin, F., D'Eletto, M., Farrace, M.G., and Piacentini, M. (2014). Transglutaminase type 2: A multifunctional protein chaperone? Mol. Cell. Oncol. *1*, e968506.

Rossin, F., D'Eletto, M., Falasca, L., Sepe, S., Cocco, S., Fimia, G.M., Campanella, M., Mastroberardino, P.G., Farrace, M.G., and Piacentini, M. (2015). Transglutaminase 2 ablation leads to mitophagy impairment associated with a metabolic shift towards aerobic glycolysis. Cell Death Differ. *22*, 408–418.

Rossin, F., Villella, V.R., D'Eletto, M., Farrace, M.G., Esposito, S., Ferrari, E., Monzani, R., Occhigrossi, L., Pagliarini, V., Sette, C., et al. (2018). TG2 regulates the heat-shock response by the post-translational modification of HSF1. EMBO Rep. *19*, e45067.

Sassano, M.L., van Vliet, A.R., and Agostinis, P. (2017). Mitochondria-Associated Membranes As Networking Platforms and Regulators of Cancer Cell Fate. Front. Oncol. *7*, 174.

Szabadkai, G., Bianchi, K., Várnai, P., De Stefani, D., Wieckowski, M.R., Cavagna, D., Nagy, A.I., Balla, T., and Rizzuto, R. (2006). Chaperone-mediated coupling of endoplasmic reticulum and mitochondrial Ca^{2+} channels. J. Cell Biol. *175*, 901–911.

Tatsukawa, H., Furutani, Y., Hitomi, K., and Kojima, S. (2016). Transglutaminase 2 has opposing roles in the regulation of cellular functions as well as cell growth and death. Cell Death Dis. *7*, e2244.

Wadhwa, R., Kaul, S.C., Ikawa, Y., and Sugimoto, Y. (1993a). Identification of a novel member of mouse hsp70 family. Its association with cellular mortal phenotype. J. Biol. Chem. *268*, 6615–6621.

Wadhwa, R., Kaul, S.C., Mitsui, Y., and Sugimoto, Y. (1993b). Differential subcellular distribution of mortalin in mortal and immortal mouse and human fibroblasts. Exp. Cell Res. *207*, 442–448.

Wieckowski, M.R., Giorgi, C., Lebiedzinska, M., Duszynski, J., and Pinton, P. (2009). Isolation of mitochondria-associated membranes and mitochondria from animal tissues and cells. Nat. Protoc. *4*, 1582–1590.

STAR★METHODS

KEY RESOURCES TABLE

REAGENT or RESOURCE	SOURCE	IDENTIFIER
Antibodies		
Mouse anti-Tubulin	Sigma	Cat#T-4026; RRID:AB_477577
Rabbit anti-TG2	Cell Signaling Technology	Cat#3557; RRID:AB_2202883
Mouse anti-TG2	Thermo Fisher Scientific	Cat#MA5-12739; RRID:AB_10985077
Mouse anti-HSP60	Enzo Life Sciences	Cat#ADI-SPA-806; RRID:AB_10617232
Mouse anti-GRP 75	Santa Cruz Biotechnology	Cat#sc-133137; RRID:AB_2120468
Rabbit anti-VDAC1	Abcam	Cat#ab15895; RRID:AB_2214787
Rabbit anti-SIGMAR1	Sigma-Aldrich	Cat#HPA018002; RRID:AB_1854802
Rabbit anti-Calnexin	Santa Cruz Biotechnology	Cat#sc-11397; RRID:AB_2243890)
Mouse anti-IP3R-3	BD Biosciences	Cat#610312; RRID:AB_397704
Goat anti-Rab 32	Santa Cruz Biotechnology	Cat#sc-169089; RRID:AB_10839200)
Mouse anti-TBK1	Santa Cruz Biotechnology	Cat#sc-52957; RRID:AB_783995
Rabbit anti-STING	Cell Signaling Technology	Cat#13647; RRID:AB_2732796
Mouse anti-Mitofusin 2	Abcam	Cat#ab56889; RRID:AB_2142629)
Mouse anti-Acyl-CoA synthetase long-chain family member 4 (FACL-4)	Santa Cruz Biotechnology	Cat#sc-365230; RRID:AB_10843105
Rabbit anti-PBR (TSPO)	Abcam	Cat#ab109497; RRID:AB_10862345
Goat anti-Mouse HRP	Bio-Rad	Cat#1721011; RRID:AB_2617113
Goat anti-Rabbit HRP	Bio-Rad	Cat# 1706515; RRID:AB_11125142
Rabbit anti-Goat HRP	Bio-Rad	Cat# 1721034; RRID:AB_2617114
Chemicals, Peptides, and Recombinant Proteins		
Carbonyl cyanide 3-chlorophenylhydrazone (CCCP)	Sigma-Aldrich	Cat#C2759
Z-DON-Val-Pro-Leu-OMe (Z-DON)	Zedira	Cat# Z006
MitoTracker Red CM-H_2XRos	Thermo Fisher Scientific	Cat# M7513
ER-Tracker Green	Thermo Fisher Scientific	Cat# E34251
Live Cell Imaging Solution	Thermo Fisher Scientific	Cat# A14291DJ
Rhod-2, AM, cell permeant	Thermo Fisher Scientific	Cat# R1245MP
Sodium cacodylate trihydrate	Sigma-Aldrich	Cat#C4945
Osmium tetroxide solution	Sigma-Aldrich	Cat#75632
Protein G PLUS-Agarose	Santa Cruz Biotechnology	Cat# sc-2002
NuPAGE LDS Sample Buffer (4X)	Thermo Fisher Scientific	Cat# NP0008
Critical Commercial Assays		
Duolink *In Situ* Red Starter Kit Mouse/Rabbit	Sigma-Aldrich	Cat# DUO92101
Duolink *In Situ* Wash Buffers, Fluorescence	Sigma-Aldrich	Cat# DUO82049
Duolink *In Situ* Detection Reagents Red	Sigma-Aldrich	Cat# DUO92008
Experimental Models: Cell Lines		
HEK293 cell line	ATCC	Cat#CRL-1573; RRID:CVCL_0045
HEK293^{TG2} cell line	D'Eletto et al., 2012	N/A
WT MEF	D'Eletto et al., 2009	N/A
KO MEF	D'Eletto et al., 2009	N/A
BOSC-23 cell line	ATCC	Cat#CRL-11270; RRID:CVCL_4401
WT MEF No target	Rossin et al., 2018	N/A
WT MEF shTG2	Rossin et al., 2018	N/A
KO MEF mTG2	This paper	N/A

(*Continued on next page*)

Continued

REAGENT or RESOURCE	SOURCE	IDENTIFIER
Experimental Models: Organisms/Strains		
Mouse: C57BL/6	The Jackson Laboratory	Cat#000664
Mouse: C57BL/6 knockout for TG2	De Laurenzi and Melino, 2001	N/A
Oligonucleotides		
Mouse TG2 forward EcoRI: 5′ gcgaattcatggcagaggagctgctcctggagagg 3′	This paper	N/A
Mouse TG2 reverse NotI: 5′ tagagcggccgcttaggccgggccgatgataacattccg 3′	This paper	N/A
Recombinant DNA		
pLPCX	Clontech Laboratories	Cat#631511
pLPCX-mTG2	This paper	N/A
Software and Algorithms		
GraphPad Prism 6.0	GraphPad Software	https://www.graphpad.com/RRID: SCR_002798
ImageJ64	https://imagej.nih.gov/ij/download.html	N/A

CONTACT FOR REAGENT AND RESOURCE SHARING

Further information and requests for resources and reagents should be directed to and will be fulfilled by the Lead Contact, Mauro Piacentini (mauro.piacentini@uniroma2.it).

EXPERIMENTAL MODEL AND SUBJECT DETAILS

Cell lines

WT and KO MEFs (murine embryonic fibroblasts) were obtained by spontaneous immortalization of fibroblasts derived from C57BL/6 mice embryos either wild-type or knockout for TG2. HEK293^{TG2} stably reconstituted with the wild-type TG2, were obtained as previously described (D'Eletto et al., 2012). To silence TG2, WT MEF was stably transfected with pLKO.1 plasmid containing an shRNA insert specific for TG2 (shTG2) or an shRNA insert that does not target any known genes from any species (no target shRNA) as previously described (Rossin et al., 2018). MEFs, HEK293 and HEK293^{TG2} were cultured in Dulbecco's modified Eagle's medium (Lonza) supplemented with 10% fetal bovine serum, 2 mM L-glutamine, 100 mg/ml streptomycin and 100 units/ml penicillin in a 5% CO2 incubator.

To induce mitochondrial damage MEF cells and HEK293 cells were incubated in full medium respectively with 20 μM and 10 μM carbonyl cyanide m-chlorophenyl hydrazone (CCCP). TG2 transamidating activity was inhibited incubating the cells with 40 μM Z-DON for 6 h.

Mice

All the procedures in mice were approved by the local Ethics Committee for Animal Welfare (Ministry of Health: 618/2015). Mice were maintained under regular housing conditions with standard access to food and drink in a pathogen-free facility.

METHOD DETAILS

Cloning of Murine TG2 gene

TG2 cDNA was obtained by polymerase chain reaction (PCR) amplification using a murine muscle cDNA library derived from C2C7 total mRNA. The construct of WT murine TG2 gene was designed to be inserted into the EcoRI and NotI sites of the pLPCX vector obtaining the pLPCX-mTG2 plasmid. The full length of murine TG2 gene was ligated into the EcoRI and NotI sites of the pLPCX vector, which was transformed and sequenced to verify the amplification efficacy.

TG2 knockout reconstitution by retrovirus infection

pLPCX-mTG2 was transfected in the Bosc 23 ecotropic packaging line using $CaCl_2$ and HBS to create high titer of ecotropic retrovirus. After 48 h, the retroviral supernatant was harvested, filtered through a 0.45 μm membrane and used to transduce KO MEF cells. For the creation of cell lines, KO MEF cells were transduced by replacing the culture medium with retroviral conditioned medium from Bosc 23 ecotropic packaging cells, in the presence of 8 μg/ml Polybrene followed by incubation for 16–18 h at 37°C. The culture medium was replaced with fresh D-MEM, and cells were grown, trypsinized, replated, and selected for puromycin resistance using

the antibiotic added to the culture medium (2 μg/ml). We had previously performed a survival curve with the antibiotic on untransfected cells to determine optimal antibiotic concentration and plating density.

Western blot analysis

Cells were collected in a lysis buffer containing 20 mM Tris-HCl pH 7.4, 150 mM NaCl and 1% Triton X-100 with protease inhibitor cocktail (Roche). Proteins were quantified with standard Bradford staining and resolved on SDS-polyacrylamide gel and transferred to a nitrocellulose membrane. Blots were blocked in 5% non-fat dry milk for 1 h at room temperature and then incubated overnight with the primary antibodies. The membranes were incubated with HRP-conjugated secondary antibody for 1 h at room temperature and the signal was detected by Immun-Star WesternC Kit (Bio-Rad Laboratories).

Subcellular fractionation

Subcellular fractionation was performed as previously described (Wieckowski et al., 2009). The procedure can be divided into 2 main steps. In the first, the cells were fractionated to obtain a crude mitochondrial fraction containing MAMs (denoted as crude mitochondria, Mc). In the second, a further purification of crude mitochondria resulted in the isolation of highly purified mitochondria (denoted as pure mitochondria, Mp) and MAMs.

All fractionation steps were carried out at 4°C. The cells were homogenized and crude mitochondrial and microsomal fractions were separated by differential centrifugation. Crude mitochondria was resuspended in the isolation buffer (250 mM mannitol, 5 mM HEPES, 0.5 mM EGTA, pH 7.4) and further separated on a 30% Percoll gradient to obtain low-density (MAM) and high-density (Mp) fractions. Aliquots were collected and analyzed by immunoblotting.

Co-Immunoprecipitation (Co-IP)

Cells were lysed in IP buffer, containing 150 mM NaCl, 50 mM Tris HCl pH 7.5, 2 mM EDTA, 1% NP-40 and freshly added protease inhibitor cocktail. An amount of 1.5 mg of proteins from cell lysates were subjected to immunoprecipitation using 2 μg of specific antibodies in combination with 80 μL of Protein G PLUS–Agarose beads, overnight at 4°C. LDS Sample Buffer 4 × containing 2.86 M 2-mercaptoethanol was added to beads and samples were boiled at 95°C for 10 min. Supernatants were analyzed by western blot. Crude mitochondria were prepared by differential centrifugation: unbroken cells, nuclei and large membranes were removed through a centrifugation at 500 g. The supernatant was further centrifugated at 9000 g. The pellet, which constituted the crude mitochondrial fraction, was resuspended in IP buffer with protease inhibitor cocktail (Roche).

1 mg of mitochondrial proteins were subjected to immunoprecipitation using specific antibodies in a combination with Protein G PLUS–Agarose. Immunoblot analysis was performed with indicated antibodies.

MAM fractions were purified and 500 μg of MAM proteins were subjected to immunoprecipitation using specific antibodies in a combination with Protein G PLUS–Agarose. Immunoblot analysis was performed with indicated antibodies.

Proximity Ligation Assays (PLA)

Cells were cultured for 24 h on coverslips coated with Matrigel or Poly-Lysine and then fixed with 4% paraformaldehyde pH 7.4 in PBS for 10 min at room temperature. Permeabilization was performed using 0.1% Triton X-100 in PBS for 10 min at room temperature. Blocking was realized with 0.1% Triton X-100 in PBS with 5% BSA for 1h at room temperature. Incubations with primary antibodies (VDAC1 and IP3R-3, 1:100 in 0.1% Triton X-100 in PBS with 5% BSA) were performed overnight at 4°C in a humidity chamber. Then, the cells were rinsed with Wash Buffer A. Next, PLUS and MINUS secondary PLA probes, both rabbit and mouse immunoglobulins diluted in 0.1% Triton X-100 in PBS with 5% BSA, were added for 1 h at 37°C. The incubation was followed by 5 min washes in two changes of Wash Buffer A. After this, the slides were incubated with the Duolink ligation mix for 30 min at 37°C and thereafter washed with two changes of Wash Buffer A for 5 min each. The Duolink amplification mix was then applied to the slides for 100 min at 37°C. Subsequently, the slides were washed twice for 10 min each time with Wash Buffer B. Nuclei were stained with DAPI and mounted on microscope slides, sealed with an anti-fading solution and examined under a Widefield microscope Zeiss Axiovert 200M. Quantification of the PLA red fluorescent dots was performed using ImageJ, on 10 sets of images acquired with the same optical settings and excluding the consideration of autofluorescence.

Transmission electron ultrastructural analysis

Liver samples were fixed with 2.5% glutaraldehyde in 0.1 M cacodylate buffer for 1 h at 4°C, and postfixed in 1% osmium tetroxide in 0.1 M cacodylate buffer. Samples were then dehydrated in graded ethanol and embedded in Epon resin. For ultrastructural analysis thin sections were stained with 2% uranyl acetate and observed under a Zeiss EM900 transmission electron microscope. Images were captured digitally with a Mega View II digital camera (SIS, Soft Imaging System GmbH, Munster, Germany).

The circumference of mitochondria, and the proportions of the mitochondrial outer membrane (OMM) associated with ER, were measured on the images using an image-processing software (analySIS 3.1; SIS). ER-OMM distance was measured considering three subsets of ER-OMM distances: closely associated (< 30 nm); between 31 and 50 nm; between 51 and 100 nm. Per each subset quantitation of the ER length adjacent to mitochondria was calculated and normalized by mitochondrial perimeter.

Ca^{2+} signaling analysis

Mitochondrial Ca^{2+} dynamics were monitored live in WT and KO MEFs and in HEK293 and HEK293^{TG2} cells with the fluorescent Ca^{2+}-indicator Rhod-2, AM. To monitor Ca^{2+} dynamics, ~1 x10^5 cells were seeded on 22 mm round borosilicate cover glasses in 6-well plates. Mitochondrial Ca^{2+}dynamics were imaged by loading cells with 5 μM Rhod-2, AM in mHBSS supplemented with 0.005% Pluronic® F-127 for 45 min at 37°C. After four washes with mHBSS, cells were further incubated at 37°C for 30 min to enhance mitochondrial uptake following de-esterification of the dye. Cover glasses were then mounted inside an Attofluor® cell chamber and bathed in mHBSS and the image acquisition was performed using a Leica TCS SP5 confocal laser/scanning microscope. Rhod-2 was excited with an Argon laser (514 nm) and laser power was kept between 1/5% to minimize photodamage. 100 μM ATP was used to induce Ca^{2+} release form the ER-stores. 15-25 cells were imaged in each experiment.

Aequorin measurements were performed as described (Bonora et al., 2013).

Imaging analysis of ER-mitochondria proximity

WT and KO MEFs were grown in DMEM containing penicillin-streptomycin and 10% FBS. 24 hours before imaging cells were passaged and plated on Nunc Lab-Tek Chambered Coverglass (Thermo Fisher 155361). Cells were incubated in growth media containing 20 nM MitoTracker and 100 nM ER-Tracker Green for 20 minutes at 37°C, from stocks prepared as per manufacturer's instructions. Cells were washed twice (5 minutes) with Live Cell Imaging Solution and then imaged in the same. Confocal imaging was performed using LEICA SP-5 inverted microscope using a 60x oil objective in a warm 37°C chamber. Images were acquired using the Leica LAS software and analyzed using ImageJ for co-localization. Merged images created from intensity normalized scans were thresholded to pick 'yellow spots' of colocalization; indicating ER-mitochondrial proximity.

QUANTIFICATION AND STATISTICAL ANALYSIS

Statistical details are provided in the figure legends. GraphPad Prism was used for statistical analysis. Image J64 software was used for densitometric analysis. Statistical significance was determined using the Student's t test or one-way ANOVA test. P value smaller than 0.05 ($p < 0.05$) was considered to be significant.